

# Confront a dilaton model with the LHC measurements

J.E. Wu<sup>1,\*</sup> and Q.S. Yan<sup>2,1,†</sup>

<sup>1</sup>*School of Physics Sciences, University of Chinese Academy of Sciences, Beijing 100039, P.R. China.*

<sup>2</sup>*Center for Future High Energy Physics, Chinese Academy of Sciences, Beijing 100049, P.R. China.*

(Dated: January 15, 2025)

We study the scalar potential of a dilaton model with local gauge conformal symmetry D(1) and investigate a couple of scenarios for the symmetry breaking mechanisms. We focus on the couplings of Higgs-weak vector bosons and Higgs self-couplings in this model and examine the LHC constraints on the parameter space. The parameter space where the discovered Higgs boson  $m_h = 125$  GeV can be dilaton dominant is identified and features of Higgs self-couplings are explored. It is found that via the measurement of Higgs pair production, the High Luminosity LHC running can either confirm or rule out the dilaton dominance.

Keywords: Weyl symmetry, dilaton, self-coupling

The Standard Model(SM) has worked quite well in accommodating high-energy data. The Higgs discovery in 2012 is a great leap for the development of particle physics [1, 2], which has found the last piece of the SM,  $H_{125}$ , and further has confirmed the pillars of the SM, such as the concepts of non-Abelian local gauge theory (Yang-Mills theory), the spontaneous symmetry breaking(SSB), and fermion mass generation via Yukawa type couplings.

It has been debated that the Higgs boson  $H_{125}$  could be composite, i.e. a scalar boson related with the some more fundamental strong-interaction dynamics, like the dilaton field of some walking gauge theories [3–8] or radion field from Randall-Sundrum model [9–13]. At low energy region, compared with the minimal Higgs model realized in the SM, such a scalar boson could couple to the rest of particles of the SM differently [14, 15]. There are quite efforts [16–19] to formulate the effective Lagrangian of such a scalar boson, which can be dubbed as the dilaton field in this work.

The question whether the discovered Higgs boson is fundamental or composite deserves continuous experimental pursuits. As pointed out by [20–22], the Higgs self-coupling measurement might be a key to address this issue. Higgs self-couplings for the pure potential part, excluding dynamic effects, are determined by the Higgs potential, and Higgs potential is one of the focus of theoretical study, since it could be related to the vacuum energy (the dark energy(DE)) and dark matter(DM)[23, 24] of our universe and could be also tightly connected to the evolution of our universe, playing important roles in phase transitions of universe, in stochastic gravitational wave productions, and in the mechanisms for baryogenesis and leptogenesis as well. Not only for the Higgs self-coupling, but also for others will give better constraints for the Higgs potential, such as  $\kappa_{V/2V}$  constraining the parameter  $\kappa_\lambda$  [25]. Obviously, a comprehensive measurement on the couplings of the Higgs boson might reveal the nature of the Higgs boson.

As it is well-known that the dilaton might related to a scaling symmetry of fundamental dynamics, which is also called as conformal symmetry introduced below. The global conformal symmetry and its breaking are important guiding principles to formulate its effective Lagrangian and its interaction with the Standard Model. The Higgs potential of the SM can be given as

$$V(\phi) = -\mu^2 \phi^\dagger \phi + \lambda(\phi^\dagger \phi)^2, \quad (1)$$

where  $\mu$  is a mass parameter and  $\lambda$  is the self-couplings of Higgs boson. It is also well-known that the SM preserves the scale symmetry if the parameter  $\mu \rightarrow 0$ . Thus it is natural to conjecture that  $H_{125}$  might be related to the pseud-Nambu Goldstone boson after the breaking of gauged conformal symmetry.

Among these constructions, we are interested in the branch of thoughts to localize the scaling symmetry [26–33]. In order to unify the gravity theory and electromagnetic theory, Weyl had introduced the local and gauged scaling symmetry, where a Weyl vector boson, which is a part of the connections, was introduced to play the role of Maxwell vector field [34]. Due to the fact that it contradicted with the atomic data, the idea was abandoned for a long time. It was revived by Dirac [35] in order to understand the physical laws from cosmological scale and atomic scale. Thus it enlighten a wealth of researches for gauge unification theory within the framework of geometry [36, 37]. Motivated by the great success of gauge theories in the SM, it is natural to apply the gauged scaling symmetry to the SM as demonstrated in the work [38], where the gravity theory is assumed to be linear. In contrast, it is known that the quadratic gravity is more natural to Weyl geometry [31, 33]. It is noticed that there exist works to explore the cosmological side of the theory which unifies the gravity and the SM, works to explore the particle physical side, especially to accommodate the Higgs data from the LHC, are currently lacking. This work is supposed to fill this gap.

In this work, we consider a dilaton model that is rooted in the geometry interpretation [28, 31, 33, 35, 37, 39] and confront the Higgs potentials of the model with the  $\kappa$  parameters of the model using the latest experi-

\* wujinger22@mails.ucas.ac.cn

† yanqishu@ucas.ac.cn

mental measurements [25] after spontaneous symmetry breaking of the local scale and electroweak symmetry. We identify the region of parameter space where  $H_{125}$  is dilaton dominant and investigate the capability of the High-Luminosity Large Hadron Collider (HL-LHC) [40] to probe this region. It is found that HL-LHC can confirm/rule out the dilaton dominance.

From the standpoint of differential geometry, the General Relativity (GR) is based on the Riemannian geometry with the metricity condition, while it can be modified to the Weyl conformal geometry (denoted by the tilded quantities) after extending it to the non-metricity property  $\tilde{\nabla}_\mu g_{\rho\sigma} = -2\omega_\mu g_{\rho\sigma}$ . The dilaton model includes a single real scalar field  $\Phi$  and a complex doublet scalar for Higgs field  $\phi^1$ , which Lagrangian can be put as given below:

$$\begin{aligned} \sqrt{-g}\mathcal{L} &= \sqrt{-\tilde{g}}(\mathcal{L}_k + \mathcal{L}_V), \\ \mathcal{L}_k &= \frac{\tilde{R}^2}{4!\xi^2} - \frac{\tilde{C}_{\mu\nu\rho\sigma}^2}{\eta^2} - \frac{1}{4g_w^2}\tilde{W}_{\mu\nu}^a\tilde{W}^{\mu\nu,a} - \frac{1}{4g_s^2}\tilde{F}_{\mu\nu}\tilde{F}^{\mu\nu} \\ &\quad + \frac{1}{2}\tilde{\nabla}_\mu\Phi\tilde{\nabla}^\mu\Phi + \tilde{\nabla}_\mu\phi^\dagger\tilde{\nabla}^\mu\phi, \\ -\mathcal{L}_V &= \frac{\rho}{4!}\Phi^4 + \frac{\alpha}{2}\Phi^2\phi^\dagger\phi + \frac{\lambda}{4}(\phi^\dagger\phi)^2 \\ &\quad + \frac{\beta}{2}\Phi^2\tilde{R} + \gamma\phi^\dagger\phi\tilde{R}. \end{aligned} \quad (2)$$

In the potential terms of  $\mathcal{L}_V$ , except three free parameters,  $\rho$ ,  $\alpha$ , and  $\lambda$ , we have introduced two parameters  $\beta$  and  $\gamma$  to describe the non-minimal couplings of scalar fields to gravity. In the kinetic terms, there are four couplings are introduced, which include  $\xi$ ,  $\eta$ ,  $g_w$ , and  $g_s$ . In total, there are 9 free parameters. To guarantee that the potential of the system has a bound below, here we assume that  $\rho > 0$  and  $\lambda > 0$  while  $\alpha$ ,  $\beta$ , and  $\gamma$  can be either positive or negative.

The squared Weyl tensor  $\tilde{C}_{\mu\nu\rho\sigma}^2$ , the Weyl scalar curvature  $\tilde{R}$  and the derivative  $\tilde{\nabla}_\mu$  of the scalar can be further expressed as the quantities of Riemannian geometry with the Weyl vector  $\omega_\mu$ <sup>2</sup>

$$\begin{aligned} \tilde{C}_{\mu\nu\rho\sigma}^2 &= C_{\mu\nu\rho\sigma}^2 + 6F_{\mu\nu}^2, \\ \tilde{R} &= R - 6(\omega_\mu\omega^\mu + \nabla_\mu\omega^\mu), \\ \tilde{\nabla}_\mu\phi &= \nabla_\mu\phi + d_\phi\omega_\mu\phi = \nabla_\mu\phi - \omega_\mu\phi, \end{aligned} \quad (3)$$

where  $\nabla_\mu$  is Riemannian derivative and the Weyl weight  $d_\phi = -1$  is given by the transformation in Eq.(4).  $C_{\mu\nu\rho\sigma}$  is the traceless part of Riemannian curvature tensor  $R_{\mu\nu\rho\sigma}$ , known as Riemannian Weyl-tensor. Ricci scalar is defined as  $R = g^{\mu\nu}R_{\mu\nu}$ , the second-rank Ricci

tensor is defined as  $R_{\mu\nu} = R_{\mu\alpha\nu}^\alpha$  and the four-rank Ricci tensor is defined as  $R_{\beta\mu\nu}^\alpha = \partial_\mu\Gamma_{\beta\nu}^\alpha - \partial_\nu\Gamma_{\beta\mu}^\alpha + \Gamma_{\gamma\mu}^\alpha\Gamma_{\beta\nu}^\gamma - \Gamma_{\gamma\nu}^\alpha\Gamma_{\beta\mu}^\gamma$ , which are connected with the Euler-Guass-Bonnet term[41, 42] showing the completeness of Eq.(2). All of them are dependent upon the metric  $g_{\mu\nu}$  which satisfies the metric compatibility and the Levi-Civita connection  $\Gamma_{\mu\nu}^\rho$  which is defined as  $\Gamma_{\mu\nu}^\rho = \frac{1}{2}g^{\rho\alpha}(\partial_\mu g_{\nu\alpha} + \partial_\nu g_{\mu\alpha} - \partial_\alpha g_{\mu\nu})$ .

The antisymmetric tensor  $\tilde{F}_{\mu\nu}$  is related to the Weyl vector field  $\omega_\mu$ , and is defined as  $\tilde{F}_{\mu\nu} = F_{\mu\nu}$  because it is torsionless. Thus, the tensor  $F_{\mu\nu}$  can be simplified as  $F_{\mu\nu} = \partial_\mu\omega_\nu - \partial_\nu\omega_\mu$ . It is also similar for  $W_\mu^a$  which denote the gauge fields (weak and hyper-charged vector fields) of the SM.

The Lagrangian is built upon not only the invariance of local gauge symmetries of the SM, but also the scale transformation in the following equation (4), which is natural to consider within the Weyl geometry.

$$\begin{aligned} g_{\mu\nu} &\rightarrow \Omega^2 g_{\mu\nu}, & g^{\mu\nu} &\rightarrow \Omega^{-2} g^{\mu\nu}, \\ \Phi &\rightarrow \Omega^{-1}\Phi, & \phi &\rightarrow \Omega^{-1}\phi, \\ \tilde{R} &\rightarrow \Omega^{-2}\tilde{R}, & \tilde{C}_{\mu\nu\rho\sigma} &\rightarrow \Omega^{-2}\tilde{C}_{\mu\nu\rho\sigma}, \\ \omega_\mu &\rightarrow \omega_\mu - \partial_\mu \ln \Omega. \end{aligned} \quad (4)$$

Such a local gauged Weyl conformal transformation is also called as  $D(1)$  symmetry, which is an Abelian type symmetry as demonstrated from this definition. It is noteworthy that the local gauge fields of the SM  $W_\mu^a$  are invariant under such a transformation.

This local gauged conformal symmetry must be broken at some energy scale. In literature, there are a few methods of conformal symmetry breaking.

- The first one is Coleman-Weinberg mechanism [43]. Although at tree-level the potential is unchanged with conformal transformation, after taking into account the quantum corrections to the Lagrangian, the conformal symmetry is broken via dimensional transmutation.
- The second method is to introduce some terms which explicitly break the conformal symmetry [44]. These terms have dimensional parameters.
- The third one is Stuckelberg mechanism, where without knowing how the conformal symmetry is broken dynamically, a pseudo-Nambu-Goldstone particle can be introduced. The Weyl vector field becomes massive after eating the this Goldstone field [30, 45, 46].

In this work, we will adopt the third method to describe the spontaneous conformal symmetry breaking. After the conformal symmetry breaking, a non-vanishing mass term of the scalar field is also generated, which provides a seed for the spontaneous symmetry breaking of EW gauge symmetry of the SM.

Apparently, there are three different energy scales in the model. One is the conformal symmetry breaking

<sup>1</sup> We separate the conception of Higgs field and  $H_{125}$  in this paper since the question we want to investigate is whether  $H_{125}$  is a Higgs.

<sup>2</sup> Although our notations most follow with [37], the general calculations fit with [31].

scale  $f_d$  which is the vacuum expectation value (VEV) of  $\Phi$ . The other is the EW symmetry breaking scale  $v$  which is the VEV of  $\phi$ . The third scale is  $f$ , which might be related to the scale of gravity. Typically, we can assume that  $f \gg f_d > v$ . For example, when the relation  $f \sim \Lambda_{pl}$  is assumed, the model can be an inflaton model as investigated by Refs.[31].

Notice that the scalar-tensor Lagrangian given in Eq.(2) is quadratic, which is a good candidate for quantum gravity. However, in order to return back to the GR, we can define a Brans-Dicke field  $\Theta$  to linearize the Lagrangian since all quadratic theory, or more generally, for modified f(R) theory, can be linearized as a BD type theory [47]:

$$\Theta^2 := \chi_D'^2 \Phi^2 + \chi_H'^2 H^2, \quad (5)$$

where  $H^2 = 2\phi^\dagger\phi$  denotes the modulus of the complex Higgs doublet. When the Brans-Dicke field develops a vacuum expectation value  $f$  ( $f^2 = \chi_D'^2 f_d^2 + \chi_H'^2 v^2 > 0$ ), the local conformal symmetry is broken and we can parametrize  $\Theta^2$  as

$$\Theta^2 := f^2 \Sigma^2, \quad (6)$$

with  $\Sigma^2 = \Theta^2 / \langle \Theta^2 \rangle = \Theta^2 / f^2$ , which is a dimensionless field. From Eq.(2), parameters  $\chi_D'^2$  ( $\chi_H'^2$ ) can be found which include  $\beta$  ( $\gamma$ ) and also  $\xi^2$  due to the linearization of the quadratic effect. In this parametrization,  $\Sigma$  plays the role of Goldstone boson and it can be eaten by the Weyl vector boson which becomes massive. By using the following gauge fixing conditions (unitary gauge)

$$\bar{g}_{\mu\nu} = \Sigma^2 g_{\mu\nu}, \quad \bar{\omega}_\mu = \omega_\mu - \partial_\mu \ln \Sigma, \quad (7)$$

where  $\bar{g}_{\mu\nu}$  and  $\bar{\omega}_\mu$  are physical fields, we can eliminate the Goldstone of conformal symmetry breaking from the Lagrangian. Thus only a scalar boson parametrized by  $\theta$  is left as a physical degree of freedom.

Generally speaking, here  $f$  includes the contribution of both  $\Phi$  and  $H$  and is dependent upon the parameters  $\chi_D'^2$  and  $\chi_H'^2$  as in [31] under the assumption that  $\chi_D'^2 \chi_H'^2 \neq 0$ .

Scenarios	$\chi_D'^2 > 0$	$\chi_D'^2 < 0$
$\chi_H'^2 > 0$	TSS1	HSS2
$\chi_H'^2 < 0$	HSS1	TSS2

TABLE I. The definition of scenarios are tabulated.

As mentioned above,  $\chi_D'^2 = \beta + k_D$  and  $\chi_H'^2 = \gamma + k_H$ , where  $k_{D/H}$  is the function based on the way to linearize the quadratic curvature term. Because the signs

of  $\beta$  and  $\gamma$  are undetermined, the signs of these two parameters should also undetermined, which means that there are four scenarios we can define ingeneral, 1) the first trigonometric scalar scenario (TSS1) with  $\chi_D'^2 > 0$  and  $\chi_H'^2 > 0$ , 2) the second trigonometric scalar scenario (TSS2) with  $\chi_D'^2 < 0$  and  $\chi_H'^2 < 0$ , 3) the first hyperbolic scalar scenario (HSS1) with  $\chi_D'^2 > 0$  and  $\chi_H'^2 < 0$ , and 4) the second hyperbolic scalar scenario (HSS2) with  $\chi_D'^2 < 0$  and  $\chi_H'^2 > 0$ . These four scenarios are tabulated in Table I.

The special parametrization methods for the final physical state  $\theta$  in these scenarios give  $\theta$  to be localized to the range  $(0, \pi/2)$ , which connects with the mixing of Higgs state and dilaton state with  $\frac{\pi}{4}$  as the demarcation. To be specific,  $\theta \rightarrow 0$  corresponds to the case where dilaton field breaks the conformal symmetry and the  $H_{125}$  is Higgs dominance, and  $\theta \rightarrow \frac{\pi}{2}$  corresponds to the case where Higgs doublet breaks the conformal symmetry and  $H_{125}$  is dilaton dominance.

Owing to the reason that the TSS2 can not produce the correct sign in the GR, we will not consider it here. Thus, we can label TSS1 as TSS for simplicity. Also it should be noticed that the parametrization is democratic for either the real scalar and the complex doublet, which means the similarity for HSS1 and HSS2. Therefore, we can just consider HSS1 without losing generality and define it as HSS in the discussion below.

In the TSS, we can parameterize doublet and singlet scalar fields by  $\chi_H^2 = \chi_H'^2 > 0$  and  $\chi_D^2 = \chi_D'^2 > 0$  into the following form

$$H^2 = \frac{f^2}{\chi_H^2} \Sigma^2 \sin^2 \theta, \quad \Phi^2 = \frac{f^2}{\chi_D^2} \Sigma^2 \cos^2 \theta. \quad (8)$$

Substituting complex and singlet fields into the Lagrangian and using the unitary gauge given in Eq.(7), we can arrive at a Lagrangian with only physical fields.

$\kappa$	TSS
$\kappa_v$	$\frac{U_t}{v} \arcsin[s]/s$
$\kappa_{m_W}$	$\kappa_v \sqrt{1 - \chi s^2}$
$\kappa_{m_h}$	$\frac{T_t}{\mu} \sqrt{1 - s^2}$
$\kappa_V$	$\kappa_v [1 - \chi s (\sqrt{1 - s^2} \arcsin[s] + s)]$
$\kappa_{2V}$	$1 - \chi [\arcsin^2[s](1 - 2s^2) + 4 \arcsin[s]s\sqrt{1 - s^2} + s^2]$
$\kappa_{3h}$	$\frac{F_t U_t}{\lambda_{SM} v} (1 - 2s^2) \sqrt{1 - s^2}$
$\kappa_{4h}$	$\frac{F_t}{\lambda_{SM}} (1 - \frac{28}{3} s^2 (1 - s^2))$

TABLE II. The  $\kappa$  parameters in TSS are listed.

The Higgs potential can be computed as given below:

$$\begin{aligned}
V &:= \frac{f^4 \rho}{4! \chi_D^4} - \frac{T_t^2 f^2}{2 \chi_H^2} \sin^2\left[\frac{\chi_H}{f} \theta'\right] + \frac{F_t f^4}{4 \chi_H^4} \sin^4\left[\frac{\chi_H}{f} \theta'\right], \\
&\approx \frac{f^4 \rho}{4! \chi_D^4} - \frac{F_t U_t^4}{4} + T_t^2 (1-s^2) h^2 + F_t U_t \sqrt{1-s^2} (1-2s^2) h^3 - \frac{F_t}{4} \left(1 - \frac{28s^2}{3} (1-s^2)\right) h^4.
\end{aligned} \tag{9}$$

In order to cast the Higgs potential into the standard form, some shorthanded parameters are defined and given below

$$\begin{aligned}
\theta' &:= \frac{f}{\chi_H} \theta = \bar{h} + h, \\
T_t^2 &:= \frac{f^2}{2\chi_D^2} \left(\frac{\rho\chi_H^2}{3\chi_D^2} - \alpha\right) > 0, \\
F_t &:= \lambda + \frac{\rho\chi_H^4}{6\chi_D^4} - \frac{\alpha\chi_H^2}{\chi_D^2} > 0, \\
\theta'_{VEV} &= \frac{f}{\chi_H} \arcsin\left[\frac{\chi_H}{f} U_t\right] := \bar{h}, \quad U_t := \sqrt{\frac{T_t^2}{F_t}}.
\end{aligned} \tag{10}$$

The full form of the Higgs potential of TSS is shown as the first line, which is periodic due to the periodicity of the trigonometric functions. While the form in the second line is obtained by using Taylor expansion. It should be pointed out that the expansion is based on  $\sin[\frac{\chi_H}{f} h]$ , not on  $\sin[\frac{\chi_H}{f} \theta']$  instead. Here  $h$  denotes  $H_{125}$  and the parameter  $U_t$  is the VEV of the trigonometric scenario of the electroweak scalar  $\sin[\frac{\chi_H}{f} \theta]$  in our model.

It is convenient to describe the Higgs couplings to the weak bosons and self-couplings in the  $\kappa$  scheme, and all the relevant  $\kappa$  are tabulated in Table II. It should be

pointed out that these  $\kappa$  parameters are characterized by two parameters, i.e.  $\chi$  and  $s$ , which are defined as given below

$$\begin{aligned}
\chi &:= 1 - \frac{\chi_H^2}{\chi_D^2} < 1, \\
s &:= \frac{\chi_H U_t}{f} > 0,
\end{aligned} \tag{11}$$

where the parameter  $\chi$  measures the breaking of democracy of scalars, it is 1 when  $\chi_H^2 \rightarrow 0$  and zero when  $\chi_H^2 = \chi_D^2$ . While the parameter  $s$  measures the percentage of VEV of Higgs contribution to  $f$ , and it is 0 when  $\chi_H \rightarrow 0$  and 1 when  $\chi_H U_t \rightarrow f$ . It's symmetric for  $s > 0$  and  $s < 0$  due to a  $Z_2$  symmetry of Higgs potential. For the sake of simplicity, we will only consider the case where  $s > 0$ .

For the HSS, scalar fields can be parametrized using  $\chi_H^2 = -\chi_H'^2 > 0$  and  $\chi_D^2 = \chi_D'^2 > 0$  as follows

$$H^2 = \frac{f^2}{\chi_H} \Sigma^2 \sin^2 \theta, \quad \Phi^2 = \frac{f^2}{\chi_D} \Sigma^2 \cosh^2 \theta. \tag{12}$$

Substituting these parametrization and using the unitarity gauge to the Lagrangian, the corresponding Higgs potential can be obtained:

$$\begin{aligned}
V &= \frac{f^4 \rho}{4! \chi_D^4} - \frac{T_h^2 f^2}{2 \chi_H^2} \sinh^2\left[\frac{\chi_H}{f} \theta'\right] + \frac{F_h f^4}{4 \chi_H^4} \sinh^4\left[\frac{\chi_H}{f} \theta'\right], \\
&\approx \frac{f^4 \rho}{4! \chi_D^4} - \frac{F_h U_h^4}{4} + T_h^2 (1+s^2) h^2 + F_h U_h \sqrt{1+s^2} (1+2s^2) h^3 + \frac{F_h}{4} \left(1 + \frac{28s^2}{3} (1+s^2)\right) h^4,
\end{aligned} \tag{13}$$

with the following parameters being defined

$$\begin{aligned}
\theta' &:= \frac{f}{\chi_H} \theta = \bar{h} + h, \\
T_h^2 &:= -\frac{f^2}{2\chi_D^2} \left(\alpha + \frac{\rho\chi_H^2}{3\chi_D^2}\right) > 0, \\
F_h &:= \lambda + \alpha \frac{\chi_H^2}{\chi_D^2} + \frac{\rho\chi_H^4}{6\chi_D^4} > 0, \\
\theta'_{VEV} &= \frac{f}{\chi_H} \operatorname{arcsinh}\left[\frac{\chi_H}{f} U_h\right] := \bar{h}, \quad U_h := \sqrt{\frac{T_h^2}{F_h}}.
\end{aligned} \tag{14}$$

Obviously, the potential of HSS possesses no periodicity, in contrast to that of the TSS. The potential can be expanded by using the Taylor expansion in term of

$\sinh[\frac{\chi_H}{f} h]$  rather than  $\sinh[\frac{\chi_H}{f} \theta']$ , which is given in the second line. One should realize that the origin of the difference for these two scenarios lies in the difference of trigonometric and hyperbolic functions.

From the Lagrangian, we can read off the  $\kappa$ 's and we present all  $\kappa$ 's for the HSS in Table III which are dependent upon two parameters  $\chi$  and  $s$  being defined below:

$$\begin{aligned}
\chi &:= 1 + \frac{\chi_H^2}{\chi_D^2} > 1, \\
s &:= \frac{\chi_H U_h}{f} > 0.
\end{aligned} \tag{15}$$

It should be emphasized that the definitions of  $\chi$  and  $s$  given in Eq.(11) for TSS and Eq.(15) for HSS are

$\kappa$	HSS
$\kappa_v$	$\frac{U_h}{v} \operatorname{arcsinh}[s]/s$
$\kappa_{m_W}$	$\kappa_v \sqrt{1 + \chi s^2}$
$\kappa_{m_h}$	$\frac{T_h}{\mu} \sqrt{1 + s^2}$
$\kappa_V$	$\kappa_v [1 + \chi s (\sqrt{1 + s^2} \operatorname{arcsinh}[s] + s)]$
$\kappa_{2V}$	$1 + \chi [\operatorname{arcsinh}^2[s](1 + 2s^2) + 4 \operatorname{arcsinh}[s]s\sqrt{1 + s^2} + s^2]$
$\kappa_{3h}$	$\frac{F_h U_h}{\lambda_{SM} v} (1 + 2s^2) \sqrt{1 + s^2}$
$\kappa_{4h}$	$\frac{F_h}{\lambda_{SM}} [1 + \frac{28}{3} s^2 (1 + s^2)]$

TABLE III. The  $\kappa$ 's in the HSS are tabulated.

different, since they have different dependence on the original theory parameters given in the Lagrangian. It should be pointed out that the parameter  $s > 0$  for TSS as in Eq. (11), whereas it also has a hidden up limit for  $s < 1$  as a result of trigonometric function. However, HSS is distinguished by its ranges from 0 to infinity. In the TSS,  $\chi$  is smaller than 1, while in the HSS,  $\chi$  is larger than 1. The  $U_t$  and  $U_h$  denote VEV of Higgs field in TSS and HSS, respectively.

In terms of the scenarios given above, we examine the LHC constraints on the couplings of this scalar. For our convenience, we use the mass of the W boson [48], the mass of the Higgs boson [49] and the coupling  $\kappa_V$  [50] to fix some free parameters. We fix  $\kappa_{m_W} = 1$  and  $\kappa_V = 1 + \delta$  (95%CL) based on the experimental results given in [50]:

$$\begin{aligned} \kappa_V &= 1 + \delta, \\ \delta &= 0.035^{+0.077}_{-0.074}, \end{aligned} \quad (16)$$

as model inputs which lead to the solutions of  $\chi$ .

After taking into account the requirement of Eq. (11)/(15) and Eq. (16), the allowed parameter space in the  $\chi - s$  plane can be found for these two scenarios, as being illustrated in Figure 1 and Figure 4, respectively. It's essential to highlight that the SM limit, i.e.  $s \rightarrow 0$ , is represented by a purple line in each of these two figures.

In Figure 2 and Figure 6, the recent experiment measurements on the Higgs trilinear self-coupling  $-1.2 < \kappa_\lambda (\kappa_{3h}) < 7.2$  (95%CL) are depicted by a dotted line only for its lower limit. In Figure 3 and Figure 7 the predicted  $\kappa_{4h}$  for TSS and HSS are shown. In Figure 5 the recent experiment measurements on the HHVV coupling  $-0.6 < \kappa_{2V} < 1.5$  (95%CL) are depicted by two dot-dashed lines.

Meanwhile, in Figure 2, Figure 5 and Figure 6, the projected precision of the HL-LHC [40] at 68% CL for  $0.85 < \kappa_{2V} < 1.19$  and  $0.52 < \kappa_\lambda < 1.50$  are also shown by two cyan lines and shallow cyan lines, respectively.

Figures 1-3 are results for TSS, and Figures 4-7 are results for HSS. Let's have a closer look at these plots.

In Figure 1, the shaded region is the allowed parameter space for TSS, where the SM limit corresponds to

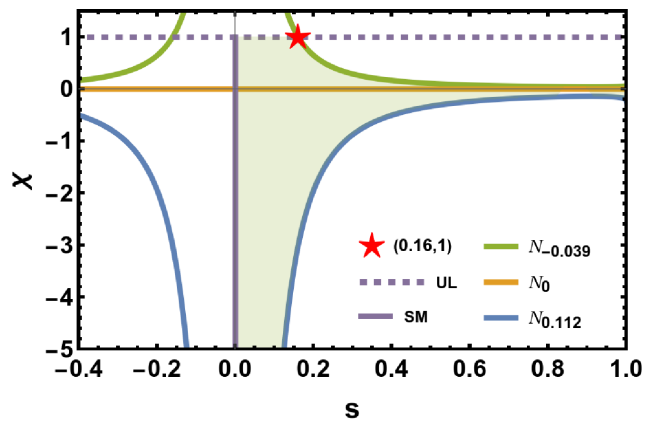


FIG. 1. Allowed parameter space by experiments for TSS in  $\chi$  and  $s$  plane is shown.

$s \rightarrow 0^+$  and  $\chi \leq 1$ . When we fix  $\kappa_{m_h} = 1$ , the predicted Higgs trilinear couplings can be determined as

$$\begin{aligned} \kappa_{3h} &= \frac{FU}{\lambda_{SM} v} (1 - 2s^2) \sqrt{1 - s^2}, \\ \xrightarrow{\kappa_{m_h}=1} & \frac{\mu^2}{\lambda_{SM} v^2} \frac{\operatorname{arcsin}[s]}{s\sqrt{1 - s^2}} (1 - 2s^2) \sqrt{1 - \chi s^2}. \end{aligned} \quad (17)$$

In particular, for TSS, we focus on the analysis of the solution  $\chi = 0$ , since it can lead an interesting relation  $\chi_D^2 = \chi_H^2$  and consequently it turns out that the difference between the predictions of TSS and the SM appear only in the Higgs self-couplings.

In Figure 2, the relationship between  $\kappa_\lambda$  and  $s$  is shown with  $s < 0.86$  bound by the experimental result. The four-pointed star marker separates the allowed parameter of  $s$  into two parts. The first part is  $0 < s < \frac{1}{\sqrt{2}}$ , where the scalar  $H_{125}$  GeV corresponds to Higgs dominance since  $H_{125}$  is mainly from complex doublet. While the second part is  $\frac{1}{\sqrt{2}} < s \leq 0.87$  ( $s \leq 0.87$  is required by the most recent  $k_{3h}$  measurement), where the scalar  $H_{125}$  GeV is dilaton boson dominant from scalar singlet mainly. Notice that  $s = \frac{1}{\sqrt{2}}$  is the maximum mixture sate for higgs and dilaton and it's hard to distinguish the higgs or dilaton dominant.

Furthermore, from Figure 2, it's observed that the HL-LHC run. is capable to confirm/rule out the parameter space of dilaton dominance. As it is known that the HL-LHC can also further improve the precision of  $\kappa_V$  (the projected precision of HL-LHC can reach to  $0.98 < \kappa_V < 1.02$ ), therefore these two measurements can cross check the parameter space of dilaton dominance.

In Figure 3, a prediction for the four-point Higgs self-coupling  $\kappa_{4h}$  is provided for TSS with  $\chi = 0$  after taking into account the experimental constraints. The dilaton dominant region  $\frac{1}{\sqrt{2}} \leq s \leq 0.87$  predicts a negative quartic Higgs self-coupling. It is remarkable that Even for the Higgs boson dominant region  $0 \leq s \leq \frac{1}{\sqrt{2}}$ , the

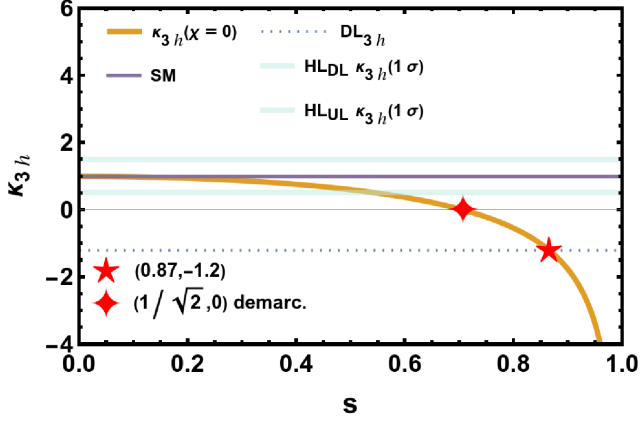


FIG. 2. The varying of  $\kappa_{3h}$  with parameter  $s$  in the TSS are shown ( $\chi = 0$ ).

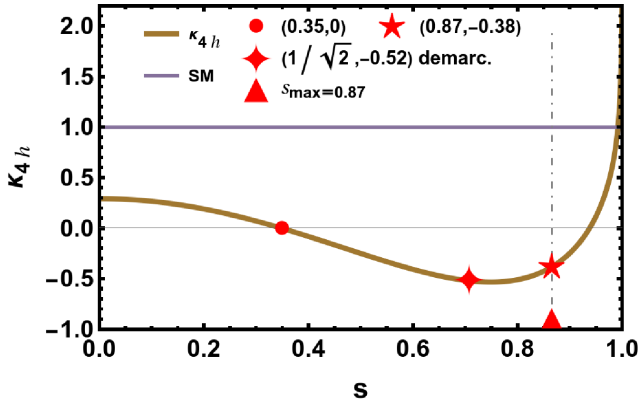


FIG. 3. The predicted  $\kappa_{4h}$  for the TSS is shown.

quartic Higgs self-coupling can be either positive or negative, and a vanishing quartic coupling is possible.

In Figure 4, the parameter space of HSS is shown in  $\chi - s$  plane, where the shaded region is allowed by Eq.(15) and Eq.(16).

In Figure 5, the measurement of  $\kappa_{2V}$  at the HL-LHC

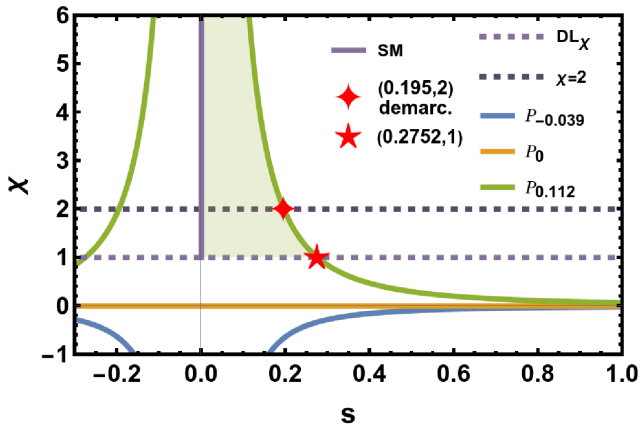


FIG. 4. Allowed parameter space in the HSS is shown.

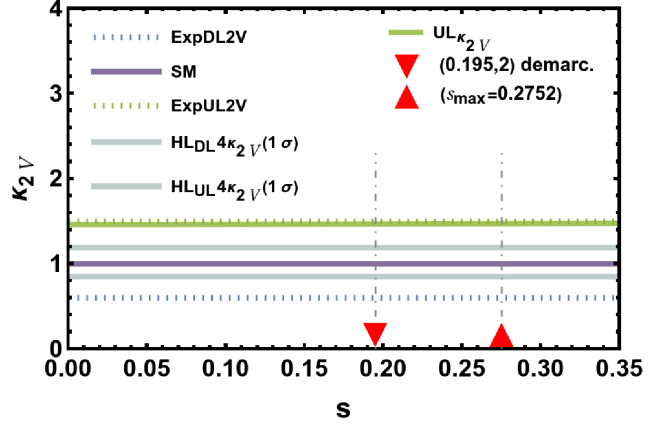


FIG. 5. The constraints to  $\kappa_{2V}$  in the HSS are shown.

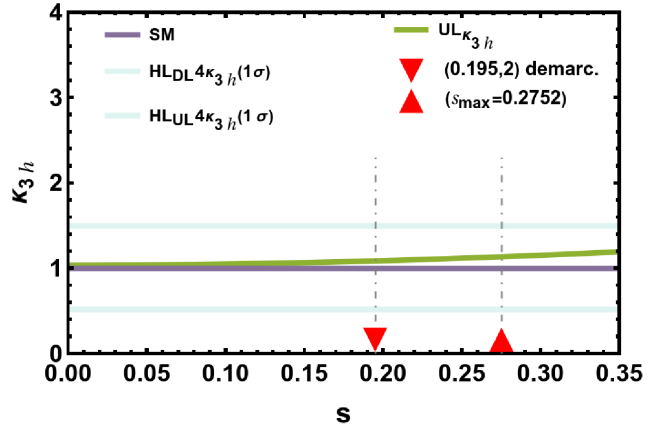


FIG. 6. The constraints to  $\kappa_{3h}$  for the HSS are shown.

is capable to probe the parameter space of HSS. In Figure 6, the measurement of  $\kappa_{3h}$  at the HL-LHC is projected and it is obvious that this measurement can not provide meaningful constraints on the allowed parameter space. In Figure 7, the predicted  $\kappa_{4h}$  is also shown, which will be difficult to be measured even at the future 100 TeV colliders [51–53]. Nonetheless, it is also found that the measurement of  $\kappa_V$  at the HL-LHC can also be improved and can reach to similar precision. In these plots, the triangle marker denotes the maximum value of  $s$  and the inverted triangle marker denotes the separation of Higgs dominance and dilaton dominance on the allowed green curve.

In Table V, we also list a few typical scalar potentials in literatures which can trigger spontaneous symmetry breaking. In Figure 8, we compare the shapes of these potentials.

In the reference [31], the Higgs potential in the SMW was found to have the following form

$$V(\sigma) = \frac{3}{2} M_p^2 \left\{ 6\lambda \sinh^4 \frac{\sigma}{M_p \sqrt{6}} + \xi^2 \left( 1 - \xi_h \sinh^2 \frac{\sigma}{M_p \sqrt{6}} \right)^2 \right\}, \quad (18)$$

where  $\sigma$  is assumed to be the Higgs boson, and  $M_p$

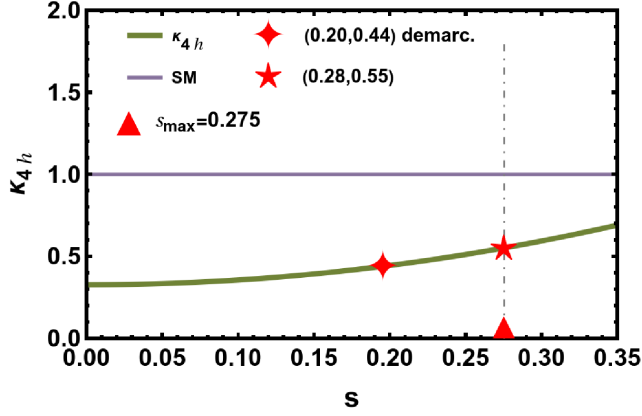


FIG. 7. The prediction of HSS for  $\kappa_{4h}$  is shown.

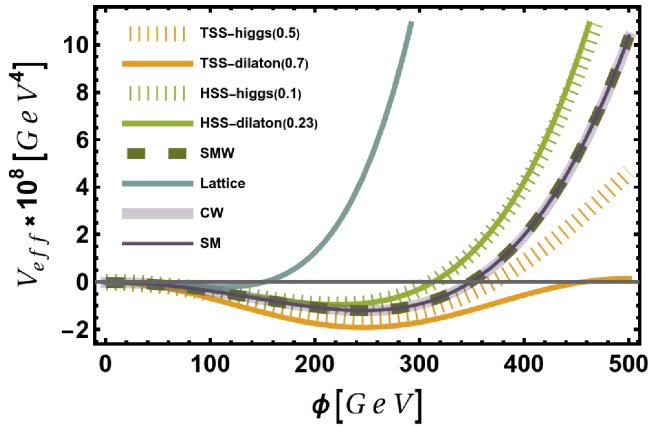


FIG. 8. The shape of Higgs potentials are demonstrated.

is the Planck energy scale. The parameters  $\xi$  and  $\xi_h$  represented two non-minimal couplings. In the limit that  $\sigma \ll M_p$ , the potential can be expanded as

$$V(\sigma) = \frac{1}{4}(\lambda - \frac{1}{9}\xi_h\xi^2 + \frac{1}{6}\xi_h^2\xi^2)\sigma^4 - \frac{1}{2}\xi_h\xi^2 M_p^2 \sigma^2 + \dots, \quad (19)$$

which takes the form of Higgs potential of the SM. In order to comply with the value of the Higgs mass and EW VEV, we choose the parameters  $\xi\sqrt{\xi_h} \sim 3.5 \times 10^{-17}$  and  $\lambda \sim \lambda_{SM}$  as shown in the second row of Table IV.

In the reference [54], in terms of scale transformation, by introducing the spurion field into the low-energy ef-

Framework	$\xi_h$	$\xi$
Particle Physics	$\xi\sqrt{\xi_h} \sim 3.5 \times 10^{-17}$ To fix the mass of $H_{125}$	
Cosmology	$10^{-3} \sim 10^{-2}$ Inflation	$10^{-9}$ CMB

TABLE IV. The typical orders of parameters in SMW[31] to accommodate experimental data are provided.

fective theory, the general dilaton potential can be of the form

$$V(\chi) = \chi^4 \sum_{n=0}^{\infty} c_n(\Delta_{\mathcal{O}}) \left(\frac{\chi}{f}\right)^{n(\Delta_{\mathcal{O}}-4)}, \quad (20)$$

where  $\chi$  represents dilaton field,  $f$  is the VEV of  $\chi$ , and  $\Delta_{\mathcal{O}}$  denotes the dimension of the operator  $\mathcal{O}$  which breaks the conformal symmetry. And the coefficients  $c_n$  depend on the dynamics of the underlying conformal field theory. In the limit  $\Delta_{\mathcal{O}} \rightarrow 4$ , the potential can be of the form

$$V(\chi) = \frac{1}{16} \frac{m^2}{f^2} \chi^4 [4 \ln \frac{\chi}{f} - 1] + \mathcal{O}(|\Delta_{\mathcal{O}} - 4|^2). \quad (21)$$

It includes the NP scale  $f$  and  $\frac{m^2}{f^2} \ll 1$  explicit breaks the conformal symmetry, which is set as  $f = 5$  TeV and  $m \sim 125.11$  GeV in order to compare and contrast with other potentials in Figure 8.

In reference [55, 56], in order to explore the dynamic of conformal symmetry breaking, an effective field theory of dilaton field is constructed by using lattice data. The effective potential of dilaton field can be cast into a form as given below

$$V(\chi) = \frac{m^2 \chi^4}{4(4-\Delta)f^2} \left[ 1 - \frac{4}{\Delta} \left(\frac{f}{\chi}\right)^{4-\Delta} \right] - \frac{N_f m_\pi^2 f_\pi^2}{2} \left(\frac{\chi}{f}\right)^y. \quad (22)$$

The last term in the potential is attributed to the contributions of light quarks, where  $m_\pi$  and  $f_\pi$  are mass and decay constant of pion fields. The parameters  $\Delta$  and  $y$  can be determined from Lattice data. By using the SU(3) YM theory with  $N_f = 8$  Dirac fermions in the fundamental representation, it was found that these two parameters can be determined by  $\Delta = 3.5$  and  $y = 2.06 \pm 0.05$  shown in the Table 1 of [55].

It is noteworthy that potentials given in Eq.(21) and Eq.(22) can also be introduced to explicitly break the local conformal symmetry of the Lagrangian in Eq.(2) as well, which belong to the second method. Here these two potentials serve as the template potentials to describe the dilaton dominance cases.

Model	Potential	$m_{H_{125}}$ (GeV)	VEV (GeV)
TSS	Eq.(9)	125.11	246.3
		125.11	246.3
HSS	Eq.(13)	125.11	221.1
		125.11	222.7
SMW [31]	Eq.(19)	125.11	246.3
CW [54]	Eq.(21)	126.15	246.8
Lattice [55, 56]	Eq.(22)	125.11	109.8
SM	Eq.(1)	125.11	246.3

TABLE V. Higgs potentials in a few typical models are provided and compared.

After choosing some parameters as given in Table V, we plot the shape of these Higgs potentials which are shown in Figure 8. For the scenarios we discuss above, we thoroughly demonstrate each possibility. The orange curves represent two TSS cases: the dotted curve is Higgs dominance with  $s = 0.5$  and the thick dotted curve is dilaton dominance with  $s = 0.7$ . Meanwhile, there are two HSS cases one for Higgs dominance with  $s = 0.1$  and the other one for dilaton dominance with  $s = 0.23$  which are shown in green curves. The potential of the SMW model is plotted by a dashed curve while the potential determined from Lattice calculation is drawn by using a darker cyan curve. A shallow purple curve is to represent the Higgs potential including Coleman-Weinberg correction. The purple curve is for the Higgs potential of the SM.

An obvious feature is that these scalar potentials can trigger spontaneous EW symmetry breaking successfully after the conformal symmetry breaking and can accommodate Higgs data, the correspondent mass of  $H_{125}$  demonstrated in the third column of Table V which is fixed at 125.11 GeV. There are a few comments in order.

- Although the VEV of HSS is different from that of the SM, it is consistent with experimental errors.
- The CW type potential shifts the mass and VEV relative to SM owing to the contribution of quantum correction.
- One special exception is the Lattice type, where the VEV is 109.8 GeV. The gap between theoretical and experimental VEV is large. It is found that if the parameter of  $m_\pi$  or  $f_\pi$  can be free, it is possible to arrive at the correct value of VEV with the compensation of the shifting mass. It is also observed that without adjusting  $f_\pi$  or  $m_\pi$ , the situation can be only slightly improved after taking into account quantum correction, i.e. the one-loop CW correction, but the shifting mass is inadequate to fill this gap.
- It should be pointed out that the potential of TSS-dilaton in Figure 8 starts to drop down after  $\phi > 500$ , which can be attributed to the oscillating behavior of the full potential given in Eq.(9).
- A remarkable character of our model is that the potentials of HSS are exponentially dependent upon  $h$  while those of TSS are periodic, which might have some different effects during phase transitions.
- Thanks to the mixing between dilaton and Higgs as given in Eq.(5), there are three scales shown up in the model, i.e.  $f$ ,  $f_d$ , and  $v$ . The association of  $f$  to the electroweak scale  $v$  and the scale for scale symmetry breaking scale  $f_d$  depends upon the parameters  $\chi_H$  and  $\chi_D$ . Hence, if  $\chi_H$  and  $\chi_D$  are large, the scale  $f$  could be much larger than  $v$

and  $f_d$ , which could lead to the supercooling phase transitions.

Although we focus on discussing the phenomenological analysis of the model with the LHC measurements, the model includes a gravity theory as demonstrated in Eq.(2) because the Lagrangian is derived from the Weyl geometry. After the scale symmetry breaking, the intrinsic scale  $f$  will give an explanation to the gravitational constant  $G$  like in Brans-Dicke theory [57]. To interpret the cosmological constant  $\Lambda$  is also one of the motivations that most models assume that  $f \sim \Lambda_{pl}$ . Meanwhile, like in the SMW [31], the cosmological constant can also be explained in the same model.

In fact, the question whether there exists a set of parameters which can accommodate both cosmology and particle physics deserves a careful study. It is noticed that actually there exists a tension in the SMW [31], where two sets of parameters for  $\xi_h$  and  $\xi$  in Eq.(19) must be introduced in order to accommodate data of cosmology and particle physics as given in Table IV. It is also found that the one for EW spontaneous symmetry breaking used in Figure 8 is different from the other one for the cosmology in order to explain inflation and CMB data. To be more precise, the VEV triggered by the set of parameters for cosmology is  $10^{13}$  GeV or so, which is much larger than that of the EW symmetry breaking in particle physics.

In this paper, we investigate the scalar sector of a dilaton model with the local gauge conformal symmetry D(1). In the model, two scenarios are identified, TSS and HSS. Furthermore, after taking into account both theoretical requirements and experimental bounds, we find the allowed parameter space of the model. Our findings support the thought that the scalar boson found at the LHC with a mass 125 GeV could be dilaton dominance and it can be further addressed by the HL-LHC. Apart from that, we also give predictions of the four-point Higgs self-coupling for TSS and also HSS showing that both of them have weaker interactions than SM prediction. In the end, we compare the potential in our model with other models showing that it can give the same Higgs mass for  $H_{125}$  based on different VEV and the distinct sharpness of TSS and HSS compared to the SM imply the thorough analysis of our model. Whether the two sets of parameters for both cosmology and particle physics can be connected when the quantum corrections [58] are taken into account deserves our future study. Meanwhile, in the model, a natural DM candidate  $\omega_\mu$  [23, 24, 45] is predicted and can be studied in our future works.

## ACKNOWLEDGMENTS

We thank Sichun Sun, Yong Tang and Tianrui Che for useful discussions. This work is supported by the Natural Science Foundation of China under the Grants No. 11875260 and No. 12275143.



- 
- [1] Georges Aad *et al.* (ATLAS), “Observation of a new particle in the search for the Standard Model Higgs boson with the ATLAS detector at the LHC,” *Phys. Lett. B* **716**, 1–29 (2012), [arXiv:1207.7214 \[hep-ex\]](#).
- [2] Serguei Chatrchyan *et al.* (CMS), “Observation of a New Boson at a Mass of 125 GeV with the CMS Experiment at the LHC,” *Phys. Lett. B* **716**, 30–61 (2012), [arXiv:1207.7235 \[hep-ex\]](#).
- [3] Bob Holdom, “Raising the sideways scale,” *Phys. Rev. D* **24**, 1441–1444 (1981).
- [4] W. A. Bardeen, C. N. Leung, and S. T. Love, “Dilaton and chiral-symmetry breaking,” *Phys. Rev. Lett.* **56**, 1230–1233 (1986).
- [5] Thomas Appelquist and L. C. R. Wijewardhana, “Chiral hierarchies from slowly running couplings in technicolor theories,” *Phys. Rev. D* **36**, 568–580 (1987).
- [6] Thomas Appelquist and Yang Bai, “A Light Dilaton in Walking Gauge Theories,” *Phys. Rev. D* **82**, 071701 (2010), [arXiv:1006.4375 \[hep-ph\]](#).
- [7] Michio Hashimoto and Koichi Yamawaki, “Technidilaton at the conformal edge,” *Physical Review D* **83** (2011), [10.1103/physrevd.83.015008](#).
- [8] Roman Zwicky, “Qcd with an infrared fixed point and a dilaton,” (2024), [arXiv:2312.13761 \[hep-ph\]](#).
- [9] Walter D. Goldberger and Mark B. Wise, “Modulus stabilization with bulk fields,” *Phys. Rev. Lett.* **83**, 4922–4925 (1999), [arXiv:hep-ph/9907447](#).
- [10] Kazumoto Haba, Shinya Matsuzaki, and Koichi Yamawaki, “Holographic technidilaton,” *Physical Review D* **82** (2010), [10.1103/physrevd.82.055007](#).
- [11] Kazumoto Haba, Shinya Matsuzaki, and Koichi Yamawaki, “Holographic techni-dilaton, or conformal higgs,” (2010), [arXiv:1003.2841 \[hep-ph\]](#).
- [12] Masafumi Kurachi, Shinya Matsuzaki, and Koichi Yamawaki, “Walking technipions in a holographic model,” *Physical Review D* **90** (2014), [10.1103/physrevd.90.095013](#).
- [13] Benedict von Harling and Géraldine Servant, “Qcd-induced electroweak phase transition,” *Journal of High Energy Physics* **2018** (2018), [10.1007/jhep01\(2018\)159](#).
- [14] Vernon Barger, Muneyuki Ishida, and Wai-Yee Keung, “Differentiating the higgs boson from the dilaton and radion at hadron colliders,” *Phys. Rev. Lett.* **108**, 101802 (2012).
- [15] P. Hernandez-Leon and L. Merlo, “Distinguishing A Higgs-Like Dilaton Scenario With A Complete Bosonic Effective Field Theory Basis,” *Phys. Rev. D* **96**, 075008 (2017), [arXiv:1703.02064 \[hep-ph\]](#).
- [16] Shinya Matsuzaki and Koichi Yamawaki, “Discovering the 125 gev techni-dilaton at the lhc,” *Physical Review D* **86** (2012), [10.1103/physrevd.86.035025](#).
- [17] Shinya Matsuzaki and Koichi Yamawaki, “Walking on the ladder: 125 gev technidilaton, or conformal higgs,” *Journal of High Energy Physics* **2015**, 1–57 (2015).
- [18] Shinya Matsuzaki and Koichi Yamawaki, “Holographic techni-dilaton at 125 GeV,” *Phys. Rev. D* **86**, 115004 (2012), [arXiv:1209.2017 \[hep-ph\]](#).
- [19] Shinya Matsuzaki and Koichi Yamawaki, “Is 125 gev techni-dilaton found at lhc?” *Physics Letters B* **719**, 378–382 (2013).
- [20] Giuseppe Degrandi, Pier Paolo Giardino, Fabio Maltoni, and Davide Pagani, “Probing the Higgs self coupling via single Higgs production at the LHC,” *JHEP* **12**, 080 (2016), [arXiv:1607.04251 \[hep-ph\]](#).
- [21] Kenneth Lane, “The Composite Higgs Signal at the Next Big Collider,” in *Snowmass 2021* (2022) [arXiv:2203.03710 \[hep-ph\]](#).
- [22] Thomas Steingasser and David I. Kaiser, “Higgs potential criticality beyond the Standard Model,” *Phys. Rev. D* **108**, 095035 (2023), [arXiv:2307.10361 \[hep-ph\]](#).
- [23] Chao-guang Huang, Dan-di Wu, and Han-qing Zheng, “COSMOLOGICAL CONSTRAINTS TO WEYL’S VECTOR MESON,” *Commun. Theor. Phys.* **14**, 373–378 (1990).
- [24] Yong Tang and Yue-Liang Wu, “Weyl Symmetry Inspired Inflation and Dark Matter,” *Phys. Lett. B* **803**, 135320 (2020), [arXiv:1904.04493 \[hep-ph\]](#).
- [25] Georges Aad *et al.* (ATLAS), “Combination of Searches for Higgs Boson Pair Production in pp Collisions at s=13 TeV with the ATLAS Detector,” *Phys. Rev. Lett.* **133**, 101801 (2024), [arXiv:2406.09971 \[hep-ex\]](#).
- [26] Kenji Hayashi, Masahiro Kasuya, and Takeshi Shirafuji, “Elementary particles and weyl’s gauge field,” *Progress of Theoretical Physics* **59**, 681–681 (1978), <https://academic.oup.com/ptp/article-pdf/59/2/681/5308006/59-2-681.pdf>.
- [27] K. Hayashi and T. Kugo, “Remarks on Weyl’s Gauge Field,” *Progress of Theoretical Physics* **61**, 334–346 (1979).
- [28] D. M. Ghilencea and Hyun Min Lee, “Weyl gauge symmetry and its spontaneous breaking in the standard model and inflation,” *Phys. Rev. D* **99**, 115007 (2019), [arXiv:1809.09174 \[hep-th\]](#).
- [29] D. M. Ghilencea, “Spontaneous breaking of weyl quadratic gravity to einstein action and higgs potential,” *Journal of High Energy Physics* **2019** (2019), [10.1007/jhep03\(2019\)049](#).
- [30] D. M. Ghilencea, “Stueckelberg breaking of weyl conformal geometry and applications to gravity,” *Phys. Rev. D* **101**, 045010 (2020).
- [31] D. M. Ghilencea, “Standard Model in Weyl conformal geometry,” *Eur. Phys. J. C* **82**, 23 (2022), [arXiv:2104.15118 \[hep-ph\]](#).
- [32] D. M. Ghilencea, “Non-metric geometry as the origin of mass in gauge theories of scale invariance,” *The European Physical Journal C* **83** (2023), [10.1140/epjc/s10052-023-11237-z](#).
- [33] D. M. Ghilencea and C. T. Hill, “Standard Model in conformal geometry: Local vs gauged scale invariance,” *Annals Phys.* **460**, 169562 (2024), [arXiv:2303.02515 \[hep-th\]](#).
- [34] H. Weyl, “Gravitation and electricity,” *Sitzungsber. Preuss. Akad. Wiss. Berlin (Math. Phys. )* **1918**, 465 (1918).
- [35] Paul A. M. Dirac, “Long range forces and broken symmetries,” *Proc. Roy. Soc. Lond. A* **333**, 403–418 (1973).
- [36] L. O’Raifeartaigh, *The dawning of gauge theory* (Princeton Univ. Press, Princeton, NJ, USA, 1997).
- [37] Friedrich W. Hehl, J.Dermott McCrea, Eckehard W. Mielke, and Yuval Ne’eman, “Metric-affine gauge the-

- ory of gravity: field equations, noether identities, world spinors, and breaking of dilation invariance,” *Physics Reports* **258**, 1–171 (1995).
- [38] Marco de Cesare, John W. Moffat, and Mairi Sakellariadou, “Local conformal symmetry in non-Riemannian geometry and the origin of physical scales,” *Eur. Phys. J. C* **77**, 605 (2017), [arXiv:1612.08066 \[hep-th\]](#).
- [39] A. Trautman, “THE GEOMETRY OF GAUGE FIELDS. (TALK),” *Czech. J. Phys. B* **29**, 107–116 (1979).
- [40] Andrea Dainese, Michelangelo Mangano, Andreas B. Meyer, Alejandro Nisati, Gavin Salam, and Mika Anton Vesterinen, eds., *Report on the Physics at the HL-LHC, and Perspectives for the HE-LHC*, CERN Yellow Reports: Monographs, Vol. 7/2019 (CERN, Geneva, Switzerland, 2019).
- [41] Shiing-Shen Chern, “A simple intrinsic proof of the gauss-bonnet formula for closed riemannian manifolds,” *Annals of Mathematics* **45**, 747–752 (1944).
- [42] Shiing shen Chern, “On the curvatura integra in a riemannian manifold,” *Annals of Mathematics* **46**, 674–684 (1945).
- [43] Sidney R. Coleman and Erick J. Weinberg, “Radiative Corrections as the Origin of Spontaneous Symmetry Breaking,” *Phys. Rev. D* **7**, 1888–1910 (1973).
- [44] Riccardo Rattazzi and Alberto Zaffaroni, “Comments on the holographic picture of the randall-sundrum model,” *Journal of High Energy Physics* **2001**, 021–021 (2001).
- [45] Hung Cheng, “Possible existence of weyl’s vector meson,” *Phys. Rev. Lett.* **61**, 2182–2184 (1988).
- [46] Henri Ruegg and Marti Ruiz-Altaba, “The Stueckelberg field,” *Int. J. Mod. Phys. A* **19**, 3265–3348 (2004), [arXiv:hep-th/0304245](#).
- [47] Salvatore Capozziello and Mariafelicia De Laurentis, “Extended Theories of Gravity,” *Phys. Rept.* **509**, 167–321 (2011), [arXiv:1108.6266 \[gr-qc\]](#).
- [48] Georges Aad *et al.* (ATLAS), “Measurement of the W-boson mass and width with the ATLAS detector using proton-proton collisions at  $\sqrt{s} = 7$  TeV,” (2024), [arXiv:2403.15085 \[hep-ex\]](#).
- [49] Georges Aad *et al.* (ATLAS), “Characterising the Higgs boson with ATLAS data from Run 2 of the LHC,” *Phys. Rept.* **11**, 001 (2024), [arXiv:2404.05498 \[hep-ex\]](#).
- [50] Georges Aad *et al.* (ATLAS), “A detailed map of Higgs boson interactions by the ATLAS experiment ten years after the discovery,” *Nature* **607**, 52–59 (2022), [Erratum: Nature 612, E24 (2022)], [arXiv:2207.00092 \[hep-ex\]](#).
- [51] Chien-Yi Chen, Qi-Shu Yan, Xiaoran Zhao, Yi-Ming Zhong, and Zhijie Zhao, “Probing triple-Higgs productions via  $4b2\gamma$  decay channel at a 100 TeV hadron collider,” *Phys. Rev. D* **93**, 013007 (2016), [arXiv:1510.04013 \[hep-ph\]](#).
- [52] Wolfgang Kilian, Sichun Sun, Qi-Shu Yan, Xiaoran Zhao, and Zhijie Zhao, “New Physics in multi-Higgs boson final states,” *JHEP* **06**, 145 (2017), [arXiv:1702.03554 \[hep-ph\]](#).
- [53] Wolfgang Kilian, Sichun Sun, Qi-Shu Yan, Xiaoran Zhao, and Zhijie Zhao, “Multi-Higgs boson production and unitarity in vector-boson fusion at future hadron colliders,” *Phys. Rev. D* **101**, 076012 (2020), [arXiv:1808.05534 \[hep-ph\]](#).
- [54] Walter D. Goldberger, Benjamín Grinstein, and Witold Skiba, “Distinguishing the higgs boson from the dilaton at the large hadron collider,” *Physical Review Letters* **100** (2008), [10.1103/physrevlett.100.111802](#).
- [55] Thomas Appelquist, James Ingoldby, and Maurizio Piai, “Dilaton potential and lattice data,” *Physical Review D* **101** (2020), [10.1103/physrevd.101.075025](#).
- [56] Thomas Appelquist, James Ingoldby, and Maurizio Piai, “Dilaton effective field theory,” (2022), [arXiv:2209.14867 \[hep-ph\]](#).
- [57] Valerio Faraoni, *Cosmology in Scalar-Tensor Gravity*, Fundamental Theories of Physics No. v. 139 (Kluwer Academic Publishers, Dordrecht ; Boston, 2004).
- [58] John F. Donoghue and Gabriel Menezes, “Inducing the Einstein action in QCD-like theories,” *Phys. Rev. D* **97**, 056022 (2018), [arXiv:1712.04468 \[hep-ph\]](#).